Acta Crystallographica Section A
Foundations of Crystallography
ISSN 0108-7673

Received 7 May 2004
Accepted 8 July 2004

Precise analysis of the components of diffraction by cylindrical crystals

Hua-Chen Hu* and Zhen Yang

China Institute of Atomic Energy, PO Box 275 (18), Beijing 102413, People's Republic of China. Correspondence e-mail: hchu@ht.rol.cn.net

A detailed quantitative analysis of the various Bragg and Laue components of the integrated reflection power ratio for cylindrical crystals, and the dependence of these components on the Bragg angle, θ_B, the reduced radius, $\tau_0 = \sigma_0\rho$, and the ratio of absorption coefficient to diffraction cross section, $\mu/\sigma_0 = \xi_0$, is presented. The result indicates that the percentage of Laue and Bragg components of the integrated reflection power ratio is larger than 50% when $\theta_B \le 20^\circ$ and $\mu\rho \le 1$, and when $\theta_B \ge 10^\circ$ and $\mu\rho \ge 5$. The reflection power ratio profile for cylindrical crystals with large $\mu\rho$ is also discussed.

1. Introduction

The geometrical boundary for diffraction from cylindrical and spherical crystals presents a difficult but important problem in the evaluation of extinction. The most widely used extinction theory, proposed by Becker & Coppens (1974*a*,*b*) (hereafter BC), approximates the diffraction mainly as Laue case, with satisfactory results up to $\mu\rho \le 2.5$. In the statistical dynamic theory of Kawamura & Kato (1983) (KK), a region with Bragg reflection is considered and a straight-line segment is used to approximate the circumference of a circle. However, the results of KK deviate considerably from those of BC when $\mu\rho \simeq 2$. On the basis of the general solution of the power transfer equations for a plane crystal under asymmetrical diffraction geometry (Hu, 1997*a*,*b*; Lipson *et al.*, 2004), the secondary extinction and diffraction behaviors in cylindrical crystals were investigated in a previous paper (Hu, 2003), hereafter referred to as SECY, in which the reflection power ratio (RPR) profile was for the first time obtained by numerical calculation, and the importance of the Bragg–Bragg reflection region wedged into the Laue–Laue zone with varying symmetry was noted. The present paper, a continuation of SECY, presents an additional quantitative investigation of the different components of the RPR profile of cylindrical crystals. Results are reported as functions of θ_B, τ_0 and ξ_0, calculated with an appropriate modification of the computer program.

2. Results and discussion

All the notations used here are the same as those in SECY. Fig. 1 shows the diffraction geometry of a cylinder at $\theta_B = 25^\circ$ and the corresponding RPR distribution curve of a crystal with a rectangular mosaic distribution. **cef** represents the Laue-entrance surface, and **fg** the Bragg-entrance and Bragg-exit surfaces. Following the notation of Saka *et al.* (1972) and SECY, the latter is referred to as BB. **ghd** represents the Laue-exit surface; all the corresponding codes are shown in Fig. 1. Point **g** with its projection on the $\sigma_0 X$ axis, *i.e.* $2\tau_0 \sin^2\theta_B$ (see footnote 4 of SECY), is the border separating the exits of the Bragg and Laue parts; the relative importance of these two parts in the RPR distribution curve depends on both θ_B and $\mu\rho$ ($\mu\rho = \xi_0\tau_0$).

Table 1 lists the integrated reflection power ratio, R_H^θ/η (IRPR), and the percentage values of the BB, BL, LB and LL contributions at θ_B = 10 and 20° for different ξ_0 and τ_0; the corresponding extinction factor, y_μ, is also reported. The

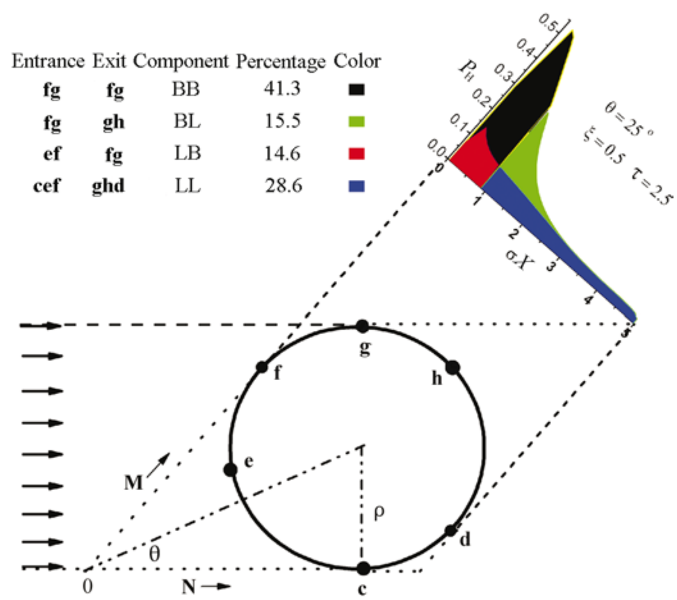

Figure 1
Diffraction geometry and reflection power ratio distribution for a cylindrical crystal with $\xi_0 = 0.5$ and $\tau_0 = 2.5$ at $\theta_B = 25^\circ$. The diffraction geometry is composed of four different components with different entrances and exits. The corresponding areas under the diffraction curve are shown in different colors.

Table 1
The IRPR, the percentages of the BB, BL, LB and LL components in the IRPR, and the secondary extinction factor y_μ for cylindrical crystals with rectangular mosaic distribution as functions of ξ_0 and τ_0 at $\theta_B = 10°$ and $\theta_B = 20°$.

$\theta_B = 10°$								$\theta_B = 20°$							
ξ_0	τ_0	IRPR	BB	BL	LB	LL	y_μ	ξ_0	τ_0	IRPR	BB	BL	LB	LL	y_μ
0	1	3.249	0.84	1.41	1.32	96.43	0.2986	0	1	3.357	5.52	7.09	6.71	80.69	0.3087
	2.5	8.840	1.59	1.99	1.86	94.56	0.1300		2.5	9.539	8.77	7.37	6.91	76.96	0.1403
	5	18.098	2.33	2.13	1.94	93.59	0.0665		5	19.985	11.35	6.23	6.05	76.38	0.0735
	10	36.627	3.16	1.89	1.68	93.27	0.0337		10	40.908	13.64	4.86	4.65	76.86	0.0376
	20	73.850	3.86	1.43	1.39	93.31	0.0170		20	83.019	15.31	3.56	3.48	77.65	0.0191
0.2	1	2.370	1.12	1.78	1.67	95.43	0.3050	0.2	1	2.477	7.06	8.27	7.83	76.84	0.3185
	2.5	4.211	3.12	3.46	3.23	90.19	0.1420		2.5	4.781	15.40	10.41	9.74	64.45	0.1598
	5	4.607	8.10	5.93	5.40	80.58	0.0850		5	5.931	30.70	11.11	10.74	47.44	0.1051
	10	3.737	25.00	9.85	8.70	56.47	0.0682		10	6.346	61.24	9.49	8.93	20.34	0.0963
	20	3.320	60.15	9.85	9.45	20.54	0.0913		20	8.143	89.82	3.82	3.65	2.72	0.1243
0.5	1	1.502	1.69	2.50	2.34	93.47	0.3166	0.5	1	1.61	9.99	10.21	9.65	70.15	0.3364
	2.5	1.610	7.38	6.89	6.4	79.33	0.1721		2.5	2.094	29.43	14.56	13.57	42.44	0.2097
	5	1.216	25.77	13.79	12.51	47.93	0.1569		5	2.223	61.87	12.73	12.2	13.19	0.2151
	10	1.152	61.39	13.80	11.92	12.89	0.2140		10	2.969	89.10	5.21	4.65	1.05	0.2669
	20	1.543	88.20	5.50	5.15	1.15	0.2646		20	4.912	97.84	1.14	1.01	0.01	0.3063
1.0	1	0.742	3.19	4.17	3.91	88.74	0.3422	1.0	1	0.849	16.56	13.57	12.82	57.05	0.3763
	2.5	0.514	19.68	13.94	12.89	53.49	0.2657		2.5	0.886	53.42	16.39	15.1	15.08	0.3434
	5	0.461	52.43	17.44	15.59	14.54	0.3427		5	1.142	83.35	8.03	7.47	1.15	0.4107
	10	0.591	82.95	8.74	7.06	1.25	0.4071		10	1.812	96.12	2.19	1.68	0.01	0.4552
	20	0.936	95.68	2.29	2.01	0.01	0.4527		20	3.257	99.07	0.53	0.41	0	0.4870
2.0	1	0.231	8.91	9.24	8.62	73.23	0.4211	2.0	1	0.323	34.02	18.37	17.25	30.36	0.4904
	2.5	0.167	45.38	19.31	17.54	17.77	0.4978		2.5	0.396	78.17	10.84	9.59	1.41	0.5710
	5	0.206	76.91	11.69	9.91	1.49	0.5687		5	0.613	93.75	3.38	2.85	0.01	0.6158
	10	0.314	93.96	3.62	2.40	0.02	0.6124		10	1.063	98.63	0.90	0.46	0	0.6435
	20	0.547	98.46	0.87	0.67	0	0.6424		20	2.005	99.68	0.22	0.13	0	0.6613
3.0	1	0.101	17.92	14.82	13.78	53.51	0.5273	3.0	1	0.173	50.77	18.70	17.4	13.11	0.6119
	2.5	0.094	62.39	16.88	14.94	5.80	0.6359		2.5	0.254	87.72	6.60	5.51	0.15	0.6873
	5	0.132	86.87	7.25	5.70	0.18	0.6844		5	0.422	96.72	1.89	1.39	0	0.7178
	10	0.215	97.05	1.93	1.02	0	0.7158		10	0.757	99.29	0.55	0.17	0	0.7356
	20	0.389	99.24	0.45	0.29	0	0.7350		20	1.456	99.84	0.11	0.05	0	0.7466
5.0	1	0.038	37.37	20.29	18.64	23.78	0.7029	5.0	1	0.084	71.87	13.63	12.36	2.09	0.7609
	2.5	0.048	80.63	10.26	8.39	0.65	0.7700		2.5	0.147	94.89	2.97	2.14	0	0.8006
	5	0.076	94.47	3.38	2.19	0	0.7990		5	0.259	98.69	0.88	0.44	0	0.8170
	10	0.132	99.00	0.76	0.24	0	0.8166		10	0.481	99.64	0.33	0.03	0	0.8258
	20	0.247	99.76	0.17	0.07	0	0.8255		20	0.942	99.99	0.04	0.01	0	0.8309

IRPR for a crystal with a rectangular mosaic distribution is calculated with equations (9) and (18) of SECY;[1] η is the standard deviation of the distribution. The number of grid points used for this calculation is $n_0 = 400$ for $\tau_0 \le 2.5$, $n_0 = 800$ for $\tau_0 = 5$ and $n_0 = 4000$ for $\tau_0 \ge 10$. For the non-absorption case, the main contribution is LL; for example, LL contributes more than 93% at $\theta_B = 10°$ and $\tau_0 \le 20$. The value of IRPR at $\theta_B = 10°$ and $\tau_0 = 20$ is 73.85. This is 6% larger than the corresponding value of 69.28 derived in §4 of SECY for the non-absorbing pure Laue case at $\theta_B = 0°$ owing to the existence of the three other components besides the LL part at $\theta_B > 0°$. Furthermore, as can be seen both from Table 1 and from Figs. 2 and 3 of SECY, the Laue components still contribute the main part to the IRPR at $\theta_B \le 20°$ and $\mu\rho \le 1$. However, when $\mu\rho$ increases, the main contribution in the IRPR gradually changes from the Laue component located beyond point **g** to the Bragg component before **g**. This change is seen both in Table 1 and in Figs. 4 and 8 of SECY. The BB component already exceeds 50% at $\theta_B \ge 10°$, $\xi_0 \ge 0.5$ and $\tau_0 \ge 10$, corresponding to $\mu\rho \ge 5$, and the IRPR rises almost linearly with increasing $\mu\rho$. BB contributes 99.7% of the total IRPR at $\theta_B \ge 10°$, $\xi_0 = 5$ and $\tau_0 = 20$. y_μ also increases with increasing BB component but, at $\theta_B = 10°$, y_μ deviates by 1.6% from the value obtained for pure Bragg geometry at $\theta_B = 90°$ and the same ξ_0 derived from equation (22) of SECY.

The interval of $\mu\rho$ between 1.5 and 3.5, where the main components of the IRPR change rapidly from the Laue to the Bragg case, is also the interval where a dip appears in the y_μ *versus* τ_0 curve (see Fig. 4 of SECY). However, such a dip is absent in the BC model (see Hu *et al.*, 2001). Moreover, BC and KK did not publish data beyond $\mu\rho = 4$ and 3, respectively, *i.e.* the region where the BB component starts to dominate. However, $\mu\rho > 3$ is not a rare case in practice; for example, the μ values of LiF, Ca_2F and Cu are 3.2, 29.0 and 47.0 mm^{-1}, respectively, for $\lambda = 1.54$ Å. Thus for $\mu\rho = 3$, the radius for the latter two samples would be limited to $\sim$0.1 mm. The values of μ are about ten times smaller for $\lambda = 0.7104$ Å, but even in this case the size of a sample would still be limited to 1 mm. For a sample with larger μ, the required size would be even smaller. Thus the y_μ values reported for larger $\mu\rho$ in SECY are not superfluous.

It is worth investigating the different values of y_μ around $\mu\rho = 2.5$ obtained by different authors. Our results (Hu *et al.*, 2001) for spherical crystals deviate by about 3.5% from the values of BC, but $\Delta y_\mu / y_\mu$ discrepancies between KK and BC as large as 14 and 17% for $y_\mu = 0.4$ and $\sin\theta_B = 0.5$ and 0.2, respectively, were reported by KK. In fact, the models used by these authors are quite different. In the mosaic BC model, the IRPR is an integration of RPR over the divergence angle, while the KK model is based on the theory of spherical waves, and the angular deviation of the domains is included in the coupling constant σ for the evaluation of the IRPR. The deviation at $y_\mu = 0.4$ may be larger than 10% simply because of the different approaches.

Since a sphere can be considered as a stack of cylindrical platelets with the same thickness but different radii, the largest being at the equator, it is obvious from Table 1 that the BB component for a sphere should be smaller than the corresponding component for a cylinder with the same radius.

[1] Since it was assumed that there is no incident beam along **fg** (Fig. 1) in the calculation of RPR of LB and part of LL for incidence along **ef**, the boundary condition Type III in equation (6) of Hamilton (1963) should be rewritten as $P_0(11) = 0$, $P_H(11) = [(1 + C_{11})P_H(01) + C_{12}P_0(01)]/(1 - C_{11})$.

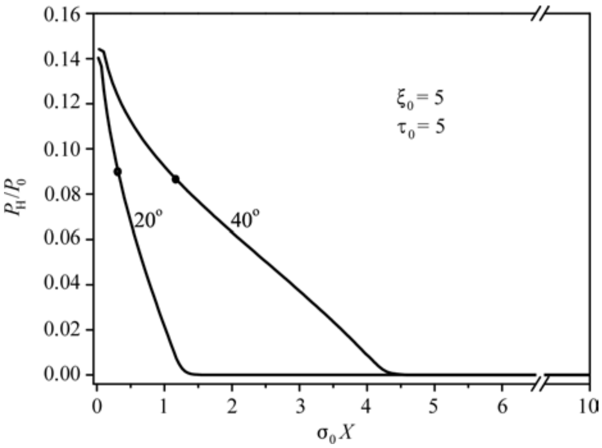

Figure 2
Power ratio distribution for absorbing cylindrical crystals with rectangular mosaic distribution at $\theta_B = 20$ and 40°. The projections of the points **g** on the $\sigma_0 X$ axis are 1.17 and 4.13 for $\theta_B = 20$ and 40°, respectively.

3. Remarks

Table 1 also clearly shows the $\sin^2\theta_B$ approximation described by SECY (p. 304); when $\mu\rho$ is large, the ratios of the IRPR values at two different θ_B values are approximately equal to the ratios of the corresponding $\sin^2\theta_B$ values. For example, at $\xi_0 = 5$ and $\tau_0 = 20$, the ratio of the IRPR values at $\theta_B = 20°$ and $\xi_B = 10°$ deviates by only 1.5% from the corresponding ratio of $\sin^2\theta_B$. This approximation can also be easily explained with Fig. 2, which shows the RPR *versus* $\sigma_0 X$ curves for $\theta_B = 20$ and 40°. Since $\mu\rho = 25$ is large, the exit beam is restricted to within the region **fg** and is essentially BB with a very small LB component. The positions of the peaks of the two RPR curves remain almost unchanged and their shapes resemble triangles; since the projection of the point **g** on the $\sigma_0 X$ axis is equal to $2\tau_0\sin^2\theta_B$, and the IRPR is proportional to the area under the curve, the $\sin^2\theta_B$ rule is evident. The RPR values corresponding to the symmetrical reflection positions for the two θ_B values indicated by dots in Fig. 2 are 0.0911 and 0.0866, respectively. They agree within 9% with the value for RPR (0.0839) calculated for the symmetrical reflection case with equation (20) of SECY. The small increase obviously comes from the extra LB component. This deviation decreases further with increasing τ_0.

However, another assumption mentioned in SECY should be modified. On p. 304 of that paper, it was assumed that, for very large $\mu\rho$, the IRPR at given θ_B and ξ_0 is approximately equal to the value from equation (21) multiplied by $\sin^2\theta_B$. This is not always true, except at $\theta_B = 90°$. The average values of RPR before point **g**, as explained in the caption of Fig. 2, are 0.0639 and 0.0647 for $\theta_B = 20$ and 40°, respectively; they contribute as much as 76.1 and 77.1% to the value of 0.0839 calculated from equation (20) of SECY. Thus, the correct assumption should be that, for a large $\mu\rho$, the IRPR for a cylinder at a given θ_B and ξ_0 is less than the value from (21) multiplied by $\sin^2\theta_B$ and the difference decreases with increasing θ_B.

The authors are grateful to Professor D. Schwarzenbach for help and valuable suggestion concerning the presentation.

References

Becker, P. & Coppens, P. (1974*a*). *Acta Cryst.* A**30**, 129–147.
Becker, P. & Coppens, P. (1974*b*). *Acta Cryst.* A**30**, 148–153.
Hamilton, W. C. (1963). *Acta Cryst.* **16**, 609–611.
Hu, H.-C. (1997*a*). *Acta Cryst.* A**53**, 484–492.
Hu, H.-C. (1997*b*). *Acta Cryst.* A**53**, 493–504.
Hu, H.-C. (2003). *Acta Cryst.* A**59**, 297–310.
Hu, H.-C., Shen, C.-W., Li, Z.-H., Qiao, Y. & Yang, B. (2001). *Chin. Phys. Lett.* **18**, 74–76.
Kawamura, T. & Kato, N. (1983). *Acta Cryst.* A**39**, 305–310.
Lipson, H., Langford, J. I. & Hu, H.-C. (2004). *International Tables for Crystallography*, Vol. C, pp. 596–598. Dordrecht/Boston/London: Kluwer Academic Publishers.
Saka, T., Katagawa, T. & Kato, N. (1972). *Acta Cryst.* A**28**, 102–113.